

# Journal of Biomedical Optics

[SPIEDigitalLibrary.org/jbo](http://SPIEDigitalLibrary.org/jbo)

## ***In vivo* deep brain imaging of rats using oral-cavity illuminated photoacoustic computed tomography**

Li Lin  
Jun Xia  
Terence T. W. Wong  
Lei Li  
Lihong V. Wang

# *In vivo* deep brain imaging of rats using oral-cavity illuminated photoacoustic computed tomography

Li Lin,<sup>a</sup> Jun Xia,<sup>a,b</sup> Terence T. W. Wong,<sup>a</sup> Lei Li,<sup>a</sup> and Lihong V. Wang<sup>a,\*</sup>

<sup>a</sup>Washington University in St. Louis, Optical Imaging Laboratory, Department of Biomedical Engineering, St. Louis, Missouri 63130, United States

<sup>b</sup>The State University of New York, University at Buffalo, Department of Biomedical Engineering, Buffalo, New York 14260, United States

**Abstract.** Using internal illumination with an optical fiber in the oral cavity, we demonstrate, for the first time, photoacoustic computed tomography (PACT) of the deep brain of rats *in vivo*. The experiment was performed on a full-ring-array PACT system, with the capability of providing high-speed cross-sectional imaging of the brain. Compared with external illumination through the cranial skull, internal illumination delivers more light to the base of the brain. Consequently, *in vivo* photoacoustic images clearly reveal deep brain structures such as the hypothalamus, brain stem, and cerebral medulla. © 2015 Society of Photo-Optical Instrumentation Engineers (SPIE) [DOI: [10.1117/1.JBO.20.1.016019](https://doi.org/10.1117/1.JBO.20.1.016019)]

Keywords: oral-cavity illumination; internal illumination; deep brain imaging; photoacoustic computed tomography; optical fiber; anatomic imaging.

Paper 140725R received Nov. 3, 2014; accepted for publication Jan. 6, 2015; published online Jan. 22, 2015.

The brain has been likened to a great stretch of unknown territory consisting of a number of unexplored continents.<sup>1</sup> Small animal brain imaging plays an important role in biomedical research. Currently, two major animal brain imaging modalities are multiphoton microscopy<sup>2,3</sup> and magnetic resonance imaging (MRI).<sup>4,5</sup> However, these imaging techniques have their own limitations. Multiphoton microscopy has a depth limit around 1 mm.<sup>6</sup> Functional MRI of small animals requires a costly high magnetic field to achieve sufficient temporal and spatial resolutions.<sup>7</sup>

As a nonionizing imaging modality, photoacoustic tomography (PAT) is gaining increasing interest in neuroimaging.<sup>8,9</sup> PAT typically utilizes a short-pulsed laser beam to create a temperature rise in biological tissue, which subsequently generates a pressure rise, causing a sound wave. The sound wave propagates through the tissue and is detected by ultrasonic transducers placed at the tissue surface. An image of the optical absorbers can then be reconstructed from the detected signals. Its hybrid nature allows PAT to image optical absorption with ultrasonically defined spatial resolution beyond the diffraction limit,<sup>10</sup> which limits the penetration capability of ballistic optical imaging such as two-photon microscopy.

Over the past few years, multiple photoacoustic (PA) brain imaging studies have been reported.<sup>11–18</sup> However, most of them focused on imaging the cortex,<sup>11,13–15,17,18</sup> mainly because of the limited light penetration depth. Thus far, only two studies on deep brain PA imaging have been reported. One used external illumination through the scalp of a dead mouse.<sup>12</sup> While some deep structures can be identified, the imaging depth was limited to intermediate layers of the brain. The dead brain also limited its usefulness in functional neural studies. The other study used an optical fiber bundle illuminating the circumference of a mouse head to acquire coronal-view images.<sup>16</sup> However, their presented image still shows strong cortex signals and the internal brain structures can barely be identified. The limited-view

half-ring detection also prevents accurate reconstruction of the cross-sectional image.

Here, we present a new light delivery scheme which allows imaging of deep brain structures in a live rat (~80 g). By inserting a multimode optical fiber with a side-illumination tip into the oral cavity of a rat, we delivered more light to the base of the brain than with conventional external illumination through the scalp. The PA signals were collected by a full-ring-array photoacoustic computed tomography (PACT) system.<sup>19,20</sup> The improved angular coverage of the full-ring ultrasonic transducer array provided faster imaging speed than a single-element ultrasonic transducer scanner<sup>12</sup> and more accurate image reconstruction than a fixed half-ring transducer array.<sup>16</sup>

Figure 1(a) shows a schematic of the oral-cavity illuminated PACT (OI-PACT) system. A tunable Ti:Sapphire laser (LT-2211A, 2004) pumped by a Q-switched Nd:YAG laser (LS-2137/2, 2004) emitted pulsed light with a 780-nm wavelength, 12-ns pulse width, and 10-Hz repetition rate. The laser beam was first condensed by two convex lenses with focal lengths of 100 mm (LB1676-B) and 25.4 mm (LB1761-B). The condensed beam, with a full-width at half-maximum of ~2 mm, was then coupled into a multimode optical fiber (2.8-mm core diameter, SGS-3.0, Fiber Optic Store) with a coupling efficiency of approximately 35%. The other end of the fiber was inserted into the rat's mouth as shown in Fig. 1(b). A 45-deg right-angle prism was attached to the fiber tip and fixed in an air chamber enclosed by transparent cladding and translucent adhesive (RTV 108, Momentive Performance Materials, Inc.). Approximately 60% of the light was reflected by the prism toward the palate; the rest of the light propagated forward and illuminated the brain stem. The fiber tip was wrapped with frosted tape (three layers, not shown in the sketch) for homogenization and protection. To quantify the illumination uniformity, we measured the light intensity around the fiber tip using a powermeter with a pinhole in front. The light

\*Address all correspondence to: Lihong V. Wang, E-mail: [lhwang@wustl.edu](mailto:lhwang@wustl.edu)

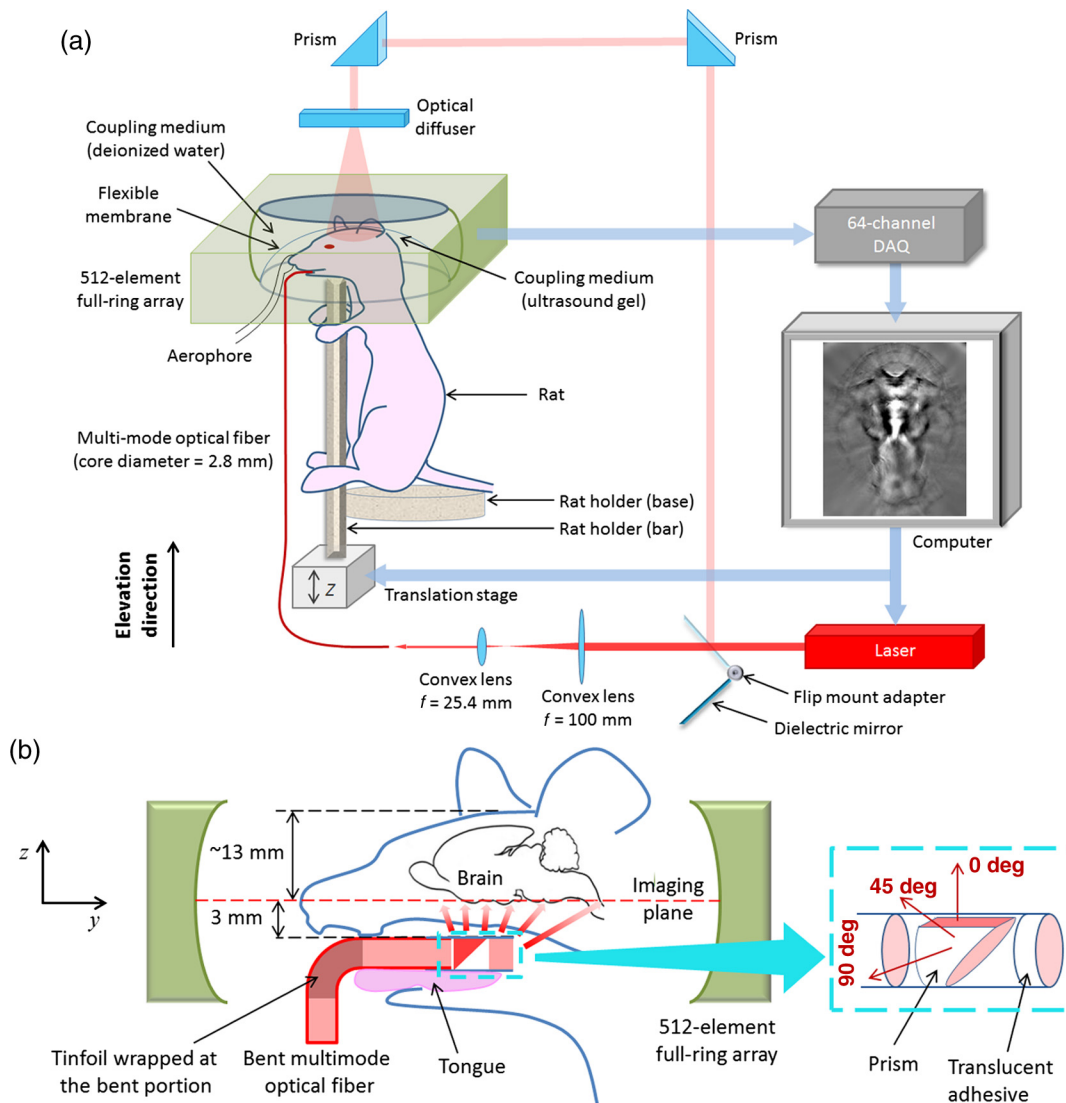


**Fig. 1** Experimental setup of the oral-cavity illuminated photoacoustic computed tomography (OI-PACT) system: (a) Schematic of the OI-PACT system. (b) Detailed view of the optical fiber tip in the rat's mouth. The origin of the z-axis was aligned with the plane 3 mm above the fiber tip.

intensities at 45 deg and 90 deg were, respectively,  $\sim 56\%$  and  $\sim 15\%$  of the intensity at 0 deg [Fig. 1(b)], where the pinhole faces the reflecting surface of the prism directly and the light intensity is the highest. The maximum light intensity at the palate surface was approximately  $20 \text{ mJ}/\text{cm}^2$ , which was below the American National Standards Institute (ANSI) limit ( $29 \text{ mJ}/\text{cm}^2$ ) at the chosen wavelength.<sup>21</sup> The 90-deg bent portion of the fiber was wrapped in aluminum foil to prevent light leakage. The total energy at the output end of the fiber was  $\sim 10 \text{ mJ}$ . To facilitate fiber insertion through the mouth, the fiber tip was lubricated with water-based lubricant (K-Y® ultragel). The insertion was smooth and should not cause any pain that might alter the neural activity.

The system also has a flippable mirror in front of the laser to alternately guide the light to the top of the rat's head for external illumination as a control [Fig. 1(a)]. The redirected light first reached an optical diffuser (EDC-10, RPC Photonics) for homogenization, and then illuminated the rat scalp from above. The light intensity was approximately  $10 \text{ mJ}/\text{cm}^2$  at

the scalp surface, also below the ANSI limit. The total energy incident on the animal was  $\sim 28 \text{ mJ}$ . The flippable mirror design allows easy switching between internal and external illuminations.

Before the experiment, the hair on the head of the rat was removed with depilatory lotion. As shown in Fig. 1(a), the rat holder consisted of a plastic base and a plastic bar as a chin holder. The rat was mounted in an upright position and was secured to the holder with paper tapes (not shown in the sketch). The bent fiber was then inserted into the rat's oral cavity and also fixed on the holder with paper tapes. We then mounted the holder on a translation stage for elevational scans. The rat was placed underneath the water tank with its scalp coupled to the flexible membrane through ultrasonic gel (Aquasonic, Parker Laboratories, Inc.) to be imaged through the membrane.

The PACT system utilized a 5-MHz (80% bandwidth) transducer array formed into a circular aperture with a 50-mm diameter.<sup>20</sup> Each element was shaped into an arc in elevation to produce an acoustic focal length of 19 mm. The combined

foci of all elements generated a central imaging region of 20-mm diameter and 1-mm thickness. Within the central imaging region, the system provided relatively uniform 0.10-mm radial (axial) resolution and <0.25-mm tangential (transverse) resolution.<sup>17</sup> The center cross section of the ultrasonic transducer array determined the imaging plane, which was 3 mm above the fiber tip [Fig. 1(b)] when we imaged the brain base. The origin of the  $z$ -axis was aligned with the plane of the brain base. For the particular rat shown here, the elevational distance from the scalp to the brain base was around 13 mm.

The data acquisition was triggered by the laser's Q-switch signal. After every other laser shot, the 8:1 multiplexers on the receiver boards forwarded the data from the transducer elements to the 64-channel acquisition board. A detailed description of the hardware can be found in previously published papers regarding the same data acquisition system.<sup>19,20</sup> The impulse responses of the transducer elements were accounted for by deconvolving the raw channel data with the PA signal generated on the transducer surface. In order to reduce artifacts caused by the acoustic heterogeneities in the rat's head, we used the simplified half-time image reconstruction algorithm,<sup>17,22</sup> which backprojected only the first half of the received data.<sup>23</sup>

To demonstrate the deep imaging capability provided by internal illumination, we imaged the deep brain structures of a healthy outbred rat (Hsd:Sprague Dawley® SD®, ~80 g). Since the Ti-Sapphire laser provided the strongest output at 780-nm wavelength, which happens to fall within the optical window, light at this wavelength was found to yield the highest quality images at depths. To investigate the advantages of internal illumination in deep brain imaging, after each measurement with fiber illumination, we also acquired corresponding control images with external illumination. Figure 2 shows a series of *in vivo* images acquired over an elevational distance of 5 mm in the brain's bottom region, with images acquired by internal illumination above [Figs. 2(a)–2(c)] and corresponding images obtained by external illumination below [Figs. 2(d)–2(f)]. We first coupled the light into the fiber for internal illumination to acquire an image [Fig. 2(a)] 1 mm below the brain base, i.e.,  $z = -1$  mm. We then flipped the mirror in front of the

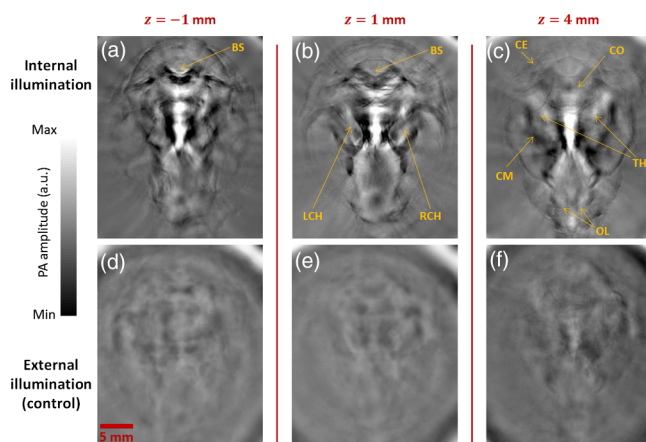


**Fig. 2** A series of images acquired at  $z = -1$  mm (a),  $z = 1$  mm (b), and  $z = 4$  mm (c), with control images at the same layers (d)–(f) acquired by external illumination through the top skull. BS, brain stem; CE, cerebellum; CM, cerebral medulla; CO, colliculus; LCH, left cerebral hemisphere; OL, olfactory lobes; RCH, right cerebral hemisphere; and TH, thalamus.

laser to redirect the light toward the top of the rat's scalp to image the same brain layer with external illumination. The acquired control image is shown in Fig. 2(d). To image the shallower brain layers, we lowered the rat by 2 mm and acquired images with both internal and external illuminations, as shown in Figs. 2(b) and 2(e), respectively. Then, to image intermediate layers of the brain, we lowered the scanning stage in three increments of 1 mm each. In Fig. 2(c), the last one of such images acquired by fiber illumination, the recognizable structures include the thalamus, cerebral medulla, colliculus, cerebellum, and olfactory lobes. The corresponding control image is shown in Fig. 2(f). Clearly, for deep brain imaging, using the same PACT data collection system and image reconstruction algorithm, internal illumination provides much clearer images than external illumination, which barely showed any recognizable structures.

Figure 3(a) shows an *in vivo* PA image of the rat brain base ( $z = 0$  mm, ventral aspect). In the image, the left and right cerebral hemispheres, brain stem, hypothalamus, and anterior cerebral artery underneath the optic chiasma are clearly visible. In addition to the brain structures, the interface between the zygoma and the muscle tissue can also be seen. After the imaging experiment, we euthanized the rat in a  $\text{CO}_2$  chamber and then dissected its brain to photograph the anatomy in ventral view [Fig. 3(b)]. The PA image and photograph agree with each other despite the fact that the release from skull confinement slightly changed the shape of the cerebral hemispheres.

With pure endogenous hemoglobin contrast and 10 times averaging, each PA image shown above was acquired over 16 s. In principle, the system can acquire an image at each laser shot by using a matched 512-channel data acquisition system. In comparison with existing illumination schemes, internal illumination delivers more light into the bottom brain and enables deep brain imaging of live rats. With external illumination, current PA imaging systems limit themselves to the imaging of brain cortex and have not been able to image the deep brain structures of any animate animals.<sup>11–18</sup>

In summary, by utilizing a fiber-transmitted internal illumination and full-view-array PACT system, we successfully

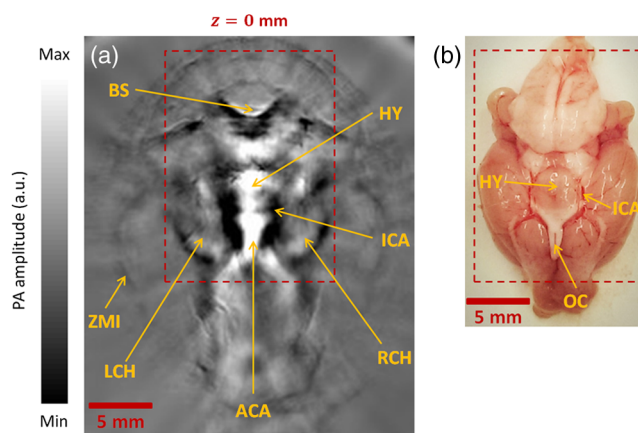


**Fig. 3** (a) *In vivo* PA image of the rat brain base ( $z = 0$  mm) acquired by OI-PACT. (b) Corresponding photograph of the anatomy of the same rat brain. ACA, anterior cerebral artery; BS, brain stem; HY, hypothalamus; ICA, internal carotid artery; LCH, left cerebral hemisphere; OC, optic chiasma; RCH, right cerebral hemisphere; and ZMI, zygomatic muscle interface.

acquired cross-sectional images of the rat's deep brain. The blood vessels under the brain, such as the anterior cerebral artery, as a part of the Circle of Willis, can potentially be investigated to study blood supply mechanisms and strokes caused by artery occlusion.<sup>24</sup> Furthermore, the capability of bottom brain imaging also enables deep brain tumor studies. By implementing external and internal illuminations simultaneously, one can potentially achieve whole brain PA imaging. This illumination method can also be expanded to kidney and prostate imaging by inserting the fiber into the colon or to lymphonodus and heart imaging via fiber illumination from the esophagus. For human subjects, the sinuses can be potentially imaged by PACT with illumination from the oral cavity.<sup>25</sup> By taking advantage of the wide choice of optical contrasts, such as near-infrared dyes<sup>26</sup> and fluorescent proteins,<sup>27</sup> different kinds of contrast mechanisms can be induced and potential benefit internally illuminated PACT for functional and molecular imaging.

### Acknowledgments

The authors would like to thank Prof. James Ballard and Dr. Junjie Yao for close reading of the manuscript. This work was supported in part by National Institutes of Health Grants DP1 EB016986 (NIH Director's Pioneer Award), R01 CA186567 (NIH Director's Transformative Research Award), R01 EB016963, and R01 EB010049. L.W. has a financial interest in Microphotoacoustics, Inc. and Endra, Inc., which, however, did not support this work.

### References

1. K. Chung et al., "Structural and molecular interrogation of intact biological systems," *Nature* **497**, 332–337 (2013).
2. T. Ragan et al., "Serial two-photon tomography for automated ex vivo mouse brain imaging," *Nat. Methods* **9**, 255–258 (2012).
3. E. E. Hoover and J. A. Squier, "Advances in multiphoton microscopy technology," *Nat. Photonics* **7**, 93–101 (2013).
4. J. P. Lerch, "Maze training in mice induces MRI-detectable brain shape changes specific to the type of learning," *NeuroImage* **54**(3), 2086–2095 (2011).
5. R. F. Kooy et al., "Brain studies of mouse models for neurogenetic disorders using in vivo magnetic resonance imaging (MRI)," *Eur. J. Hum. Genet.* **9**, 153–159 (2001).
6. D. Kobat et al., "In vivo two-photon microscopy to 1.6-mm depth in mouse cortex," *J. Biomed. Opt.* **16**(10), 106014 (2011).
7. D. H. Turnbull et al., "MRI in mouse developmental biology," *NMR Biomed.* **20**, 265–274 (2007).
8. L. V. Wang, "Multiscale photoacoustic microscopy and computed tomography," *Nat. Photonics* **3**(9), 503–509 (2009).
9. L. V. Wang and S. Hu, "Photoacoustic tomography: in vivo imaging of organelles to organs," *Science* **335**, 1458–1462 (2012).
10. L. V. Wang and H. Wu, *Biomedical Optics: Principles and Imaging*, p. 283, John Wiley & Sons Inc., Hoboken, New Jersey (2007).
11. X. Wang et al., "Non-invasive laser-induced photoacoustic tomography for structural and functional in vivo imaging of the brain," *Nat. Biotechnol.* **21**(7), 803–806 (2003).
12. X. Wang et al., "Three-dimensional laser-induced photoacoustic tomography of mouse brain with the skin and skull intact," *Opt. Lett.* **28**(19), 1739–1741 (2003).
13. G. Ku et al., "Imaging of tumor angiogenesis in rat brains in vivo by photoacoustic tomography," *Appl. Opt.* **44**(5), 770–775 (2005).
14. J. Laufer et al., "Three-dimensional noninvasive imaging of the vasculature in the mouse brain using a high resolution photoacoustic scanner," *Appl. Opt.* **48**(10), D299–D306 (2009).
15. E. W. Stein et al., "Noninvasive, in vivo imaging of the mouse brain using photoacoustic microscopy," *J. Appl. Phys.* **105**(10), 102027 (2009).
16. D. Razansky et al., "Volumetric real-time multispectral optoacoustic tomography of biomarkers," *Nat. Protoc.* **6**(8), 1121–1129 (2011).
17. J. Xia et al., "Whole-body ring-shaped confocal photoacoustic computed tomography of small animals in vivo," *J. Biomed. Opt.* **17**(5), 050506 (2012).
18. J. Yao et al., "Noninvasive photoacoustic computed tomography of mouse brain metabolism in vivo," *NeuroImage* **64**, 257–266 (2013).
19. J. Xia et al., "Three-dimensional photoacoustic tomography based on the focal-line concept," *J. Biomed. Opt.* **16**(9), 090505 (2011).
20. J. Gamelin et al., "A real-time photoacoustic tomography system for small animals," *Opt. Express* **17**(13), 10489–10498 (2009).
21. American National Standards Institute, *American National Standard for the Safe Use of Lasers*, Laser Institute of America, Orlando, Florida (2000).
22. M. A. Anastasio et al., "Half-time image reconstruction in thermoacoustic tomography," *IEEE Trans. Med. Imaging* **24**(2), 199–210 (2005).
23. M. Xu and L. V. Wang, "Universal back-projection algorithm for photoacoustic computed tomography," *Phys. Rev. E* **71**(1), 016706 (2005).
24. D. Purves et al., *Neuroscience*, 2nd ed., Sinauer Associates Inc., Sunderland, Massachusetts (2001).
25. U. Mahmood et al., "Near-infrared imaging of the sinuses: preliminary evaluation of a new technology for diagnosing maxillary sinusitis," *J. Biomed. Opt.* **15**(3), 036011 (2010).
26. M. L. Li et al., "Simultaneous molecular and hypoxia imaging of brain tumors in vivo using spectroscopic photoacoustic tomography," *Proc. IEEE* **96**(3), 481–489 (2008).
27. G. S. Filonov et al., "Deep-tissue photoacoustic tomography of a genetically encoded iRFP probe," *Angew. Chem., Int. Ed.* **51**(6), 1448–1451 (2012).

**Li Lin** is currently a PhD student at Washington University in St. Louis, under the tutelage of Dr. Lihong V. Wang. He earned his master's degree at the University of Pennsylvania in 2013 and a bachelor's degree at Tianjin University in 2011. His research focuses on photoacoustic tomography and microscopy.

**Jun Xia** earned his PhD degree at the University of Toronto in 2010 and did his postdoctoral training at Washington University in St. Louis, under the mentorship of Dr. Lihong V. Wang. He is currently an assistant professor at SUNY Buffalo. His research interests are the development of novel biomedical imaging techniques including photoacoustic imaging and ultrasonic imaging.

**Terence T. W. Wong** received the BEng (first-class honors) degree in biomedical engineering and MPhil degree in electrical and electronic engineering, both from the University of Hong Kong, in 2011 and 2013, respectively. He is now a PhD candidate in biomedical engineering at Washington University in St. Louis. His past research interests include implementing high-resolution ultrafast imaging by optical time-stretch technique. He is now working on both photoacoustic microscopy and computed tomography for biomedical applications.

**Lei Li** earned his bachelor's and master's degrees from Harbin Institute of Technology, China, in 2010 and 2012, respectively. Now he is working as a graduate research assistant under the tutelage of Dr. Lihong Wang at Washington University. His current research focuses on photoacoustic microscopy and tomography, especially to improve the photoacoustic imaging speed and to apply it to brain functional and structural imaging.

**Lihong V. Wang** earned his PhD degree at Rice University, Houston, Texas, United States. He currently holds the Gene K. Beare Distinguished Professorship of Biomedical Engineering at Washington University in St. Louis. He has published 400 peer-reviewed journal articles and delivered 400 keynote, plenary, or invited talks. His Google Scholar h-index and citations have reached 92 and over 34,000, respectively.